Chapter 3

Electrochemical Growth of Mesoporous Au NPs Film as High Surface Area Material

In this chapter, we show that using a simple template free electrodeposition process, it is possible to obtain dense mesoporous gold film on a gold surface possessing good adhesion, large surface area and mechanical integrity. The deposition was carried out using KCl as a supporting electrolyte and thiol as a stabilizer. We have electrodeposited the Au NPs in the presence of thiols such as decanethiol and 11-mercaptoundecanoic acid. The deposition was carried out with and without reducing agent such as $NaBH_4$. During the deposition Au NPs are also formed in the solution as described in the previous chapter. The measured electrochemically-active true surface area of the film prepared by this method is the highest reported for mesoscopic gold surface till now. The real surface area also increases with increasing time of deposition showing its potential for scalability. The mesoporous surface was characterized by scanning electron microscopy (SEM), atomic force microscopy (AFM), X-ray diffraction (XRD) and cyclic voltammetry (CV). The AFM and SEM images confirm the formation of porous film formed by gold nanoparticles on the surface. We have studied the electron transfer reactions of $K_4[Fe(CN)_6]$ and $[Ru(NH_3)_6]Cl_3$ at the Au NP modified surfaces using cyclic voltammetry. The high surface area gold nanoparticles deposited cathode surfaces were investigated for oxidation of dopamine and glucose in the presence of interferences. The mesoporous gold surfaces were also shown to posses high electrochemical double layer capacitance. We also observe significant enhancement in hydrogen evolution rate indicating its potential as a hydrogen evolution catalyst.

3.1 Introduction

Deposition of synthesized nanoparticles onto solid surfaces without affecting their properties remains a challenge. Supported noble metal catalysts with particle sizes down to a few nanometers are widely used for many applications. The important process in a heterogeneous catalytic reaction is the interaction of the chemical reactants with surface sites of the catalyst. This interaction depends strongly on the surface properties of the catalyst which includes

a) Large surface area-to-volume ratio
b) High surface concentrations of corner and edge atoms
c) Low coordination numbers of surface atoms
d) Unique electronic properties

The basic relationship between the surface area to volume ratio and the diameter of nanoparticles is based on spherical model for gold nanoparticles. As the size of the particle approaches a few nm, both surface area to volume ratio and surface to bulk atom ratio dramatically increases. For the nanoparticles of ~ 1nm size, more than ~ 70% atoms are at corners or edges. This aspect is important because chemisorptions is highly dependent on the atomic scale surface morphology. Haruta discovered unprecedented catalytic activity and specificity of the nanometer size gold nanoparticles. Bulk gold is chemically inert and considered as a poor catalyst. However, the catalytic activity of gold is manifested when the size of the nanoparticle reduces below 10 nm [1-2]. The sensors fabricated from the nanoparticles, and thin films comprising of nanostructures show interesting characteristics [3]. Knowledge of nano-material synthesis and nano-structured thin film deposition are fundamental for the development of nanotechnology enabled sensors and their sensitive layers. For applications in a sensing system, they may be suspended in liquid or gas phase (e.g. colloidal suspensions) or they may form ordered arrays on the surface of the transducer. The organization of such nanoparticles on substrates is therefore, an important leap forward in the development of the sensors.

The mesoporous metal thin films on solid supports find several technological applications as materials for catalysis, fuel cells, solar cells, microelectronics, supercapacitors, sensors, and medical diagnostics [4-7]. However, the realization of high surface area mesoporous metal coatings on conductive surfaces poses several problems which are not trivial. One of the early reports of the formation of a high surface area mesoporous coating is by electrochemical deposition in a lyotropic liquid crystalline phase as a template to produce ordered porous films of platinum possessing high specific surface area, well-defined long-range porosity, and good mechanical and electrochemical stability [4]. The method involves electrodeposition of the required metal through the channels provided by the template in the liquid crystal electrolyte to access the conductive substrate. This is a general synthetic scheme for forming metal films containing a lattice of periodic channels with nanometer dimensions. Ordered porous mesoscale structures of Pt were synthesized by Warren et al. from ligand stabilized Pt nanoparticles loaded

in self-assembled block copolymers acting as templates [6]. The frequently used method of preparing 2D and 3D nanostructures of gold is by the process of dealloying where an alloy of Au is treated in a suitable medium to preferentially etch away the alloying metal such as Ag, Al, and Hg, producing a mesoporous structure of gold [8-11]. This method is quite versatile and has generated renewed interest in mesoporous films by expanding their potential applications. However, this method results in a huge wastage of one of the metals and difficulties in obtaining highly pure materials due to inevitable contamination.

We discuss here a simple and effective alternative method of preparing a mesoporous thin film of gold comprised of nanoparticles on a gold substrate by utilizing the unique affinity of the sulfhydryl group to gold [12] and its inhibitory role in limiting the growth of nanoparticles. We have in the previous chapter described an electrochemical method of synthesizing monolayer protected clusters (MPCs) of alkanethiols [13]. In this method, gold dissolves anodically in a 1:1 ethanol-water mixture containing 1% by weight of $NaBH_4$, 10 mM decanethiol, and 1 M KCl. The dissolved gold ions form a chloroaurate complex in the solution, which is subsequently reduced by $NaBH_4$ in the electrolyte to produce thiol stabilized gold nanoparticles of about 1-3 nm in size. This is a simple one-step *in situ* method of preparation of MPCs in the solution, which can then be extracted to a toluene medium and purified. We also demonstrate that the thiol stabilized gold nanoparticles could be produced in the solution even in the absence of $NaBH_4$, since, in that event, ethanol can act as the reducing agent.

In this chapter, we extend the above method and show that the nanoparticles can be grown on the cathode surface as a mesoporous coating, in addition to the formation of nanoparticles in the solution. The nanoparticles grown cathode surface shows very high surface area. The real surface area increases with increasing time of deposition showing its potential for scalability. The surface was characterized by scanning electron microscopy (SEM), atomic force microscopy (AFM), X-ray diffraction (XRD) and cyclic voltammetry (CV). The AFM and SEM images confirm the formation of porous film formed by gold nanoparticles on the surface. We have studied the electron transfer reactions of $K_4[Fe(CN)_6]$ and $[Ru(NH_3)_6]Cl_3$ at the Au NP modified surfaces using cyclic voltammetry. The high surface area gold nanoparticles deposited cathode surfaces were shown to catalyze electro-oxidation of dopamine and glucose. Finally, the Au NPs coated surfaces were also shown to posses very high double layer capacitance arising out of large real surface area and also as a hydrogen evolution catalyst.

3.2 Experimental Section

3.2.1 Chemicals

All of the chemical reagents used in this study were analytical grade (AR) reagents. Sodium borohydride (Aldrich), KCl (Merck), Decanethiol (Aldrich), 11-Mercaptoundecanoic acid (Aldrich), Ethanol (Merck), Toluene (Merck) were used as received. Millipore Milli-Q water having resistivity 18 MΩ cm was used to prepare all the solutions.

3.2.2 Surface Characterization

Scanning electron microscopy (SEM) characterization was carried out using a JEOL JSM- 840A model instrument with an energy dispersive X-ray (EDAX) attachment. Atomic force microscopy (AFM) studies were conducted using a Pico plus (Molecular Imaging) instrument in ac mode (tapping mode) at a frequency of 175 kHz with a cantilever of n+-silicon of type PPP-NCL-50 from nanosensors, USA. The images shown here were corrected for plane tilt using scanning probe image processor (SPIP) software (Image Metrology, Denmark). Surface X-ray diffraction (XRD) measurements of surfaces coated with Au NPs were carried out using an Ultima X-ray diffractometer using Cu Kα radiation with a wavelength of 1.540 Å in grazing angle mode. The 2θ values were varied from 10-90°.

3.2.3 Electrochemical Instrumentation

The electrolysis was carried out using an EG&G potentiostat (model 263 A) interfaced to a computer through a GPIB card (National Instruments). This was used to control the current in a chronopotentiometry mode during the electrodeposition in a two electrode configuration. During the cyclic voltammetry (CV) studies, the potentiostat was used in a normal three-electrode configuration with a platinum counter electrode and a saturated calomel reference electrode.

3.2.4 Gold Substrate Used for Deposition

We have used a 99.9% pure gold wire of 0.5 mm diameter and 5 mm exposed length as a sacrificial anode and a gold disk of area 0.002 cm^2 obtained by sealing a 0.5 mm diameter gold wire (Arora- Mathey) in soda lime glass as a cathode. The electrodeposited samples were used for further electrochemical studies. We have also used the film coated on evaporated gold on glass (0.2 cm^2) for surface characterization studies such as SEM, EDAX, AFM, and XRD.

3.2.5 Electrode Pretreatment

Immediately before use, the gold wire electrode was polished with emery papers of grade 800 and 1500, respectively, followed by polishing in aqueous slurries of progressively finer alumina of sizes ranging from 1.0 to 0.3 to 0.05 μm on a microcloth. After this, the electrode was ultrasonicated in Millipore Milli-Q water to remove alumina particles. Then, it was cleaned in a "piranha" solution, which is a mixture of 30% H_2O_2 and concentrated H_2SO_4 in 1:3 ratio. The polished gold wire electrode was thoroughly cleaned in distilled water followed by rinsing in Millipore Milli-Q water. This electrode is subjected to potential cycling between -0.5 and 1.4 V at a scan rate of 200 mV s^{-1} in 0.1 M H_2SO_4 for about 20 cycles to effect electrochemical cleaning.

3.2.6 Electrodeposition of the Mesoporous Gold

An aqueous solution of 1M KCl in water, and 20 mM MUA or 20 mM DT in ethanol are mixed in equal proportion and stirred with a magnetic stirrer. The resulting clear solution was used as the electrolyte. The Au NPs film was deposited in the presence of $NaBH_4$ along with MUA and KCl. The gold wire acts as an anode as well as the working electrode, while the gold disk or evaporated gold on the glass substrate acts as a cathode and the counter electrode in a two-electrode configuration. A distance of about 5 mm separates these two electrodes. The electrochemical dissolution of the gold wire and the simultaneous deposition of mesoporous gold on the cathode were carried out under constant current in a chronopotentiometry mode at room temperature of 25 °C. The electrolyte was stirred by means of a magnetic stirrer during the deposition. The experiments were conducted at constant anodic current densities of 0.1, 0.2, 0.3, 0.4, and 0.5 A cm^{-2} for 30 min durations. The dissolution of gold is accompanied by evolution of gases on both the electrodes due to the electrolysis of water. Therefore, the electrochemical cell should have openings on the cell close to the electrodes to allow the gases to escape. Simultaneously an intense black colored deposit was noted over the gold surface, signifying the formation of a film of Au NPs on the cathode surface. The electrolysis was continued for different timings such as 30, 60, and 90 minutes. The amount of gold dissolved in an hour from the anode wire is 3.5 mg, while the deposited mass on the cathode was 1.6 mg cm^{-2}.

3.3 Results and Discussions

3.3.1 SEM Studies

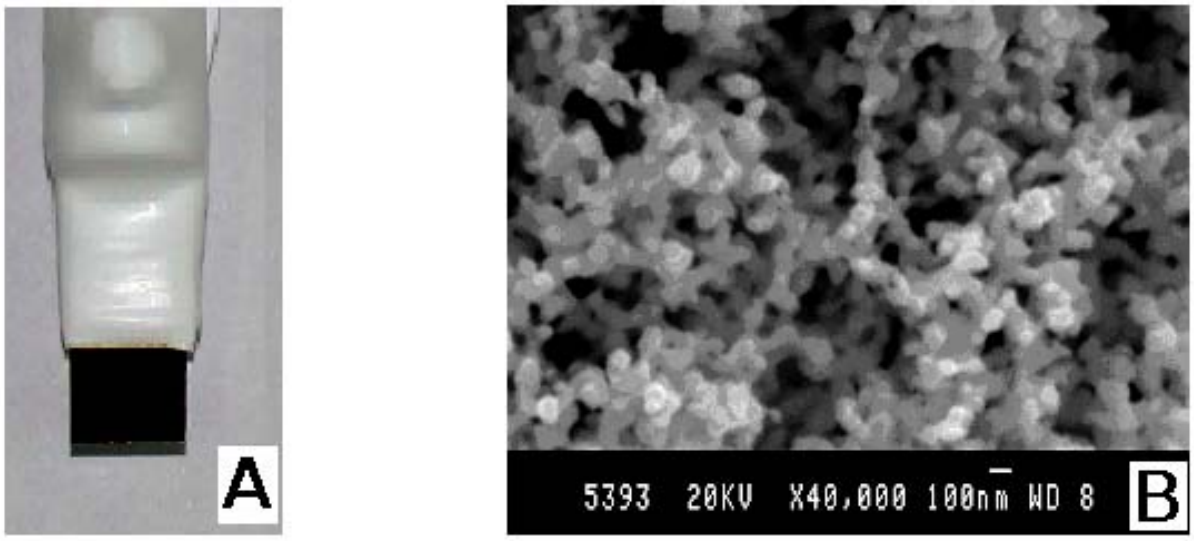

Figure 1. (A) Nanoparticles coated surface for 30 minutes (B) SEM image of the electrochemically grown Au NPs surface using MUA and KCl.

The SEM studies were conducted by depositing Au NPs on evaporated gold on glass. Figure 1A shows the sample coated with the mesoporous gold film for 30 minutes. The adhesion of the mesoporous gold on the surface was good and the film maintained its mechanical integrity during the course of several electrochemical experiments, unless scratched or abraded. Figure 1B shows the representative SEM image of the mesoporous Au on gold for 60 minutes of deposition time. The porous structure formed by the nanoparticles is clearly seen on the surface. The surface consists of random network of the interconnected grains. Figure 2 presents the SEM images of the samples deposited for 30, 60 and 90 minutes durations. The density of the film as expected, increases with time of deposition. Figure 3 shows the EDAX of the Au NPs deposited for 30 minutes duration and the data are presented in the table 1. This shows that the 94.5 % surface deposited with gold. In addition to the gold there are some electrolytes residues which are formed Au NPs film. The SEM image of Figure 4 shows the Au film grown in the presence of MUA, KCl, and $NaBH_4$. The deposited nanoparticles form dense clusters in several regions.

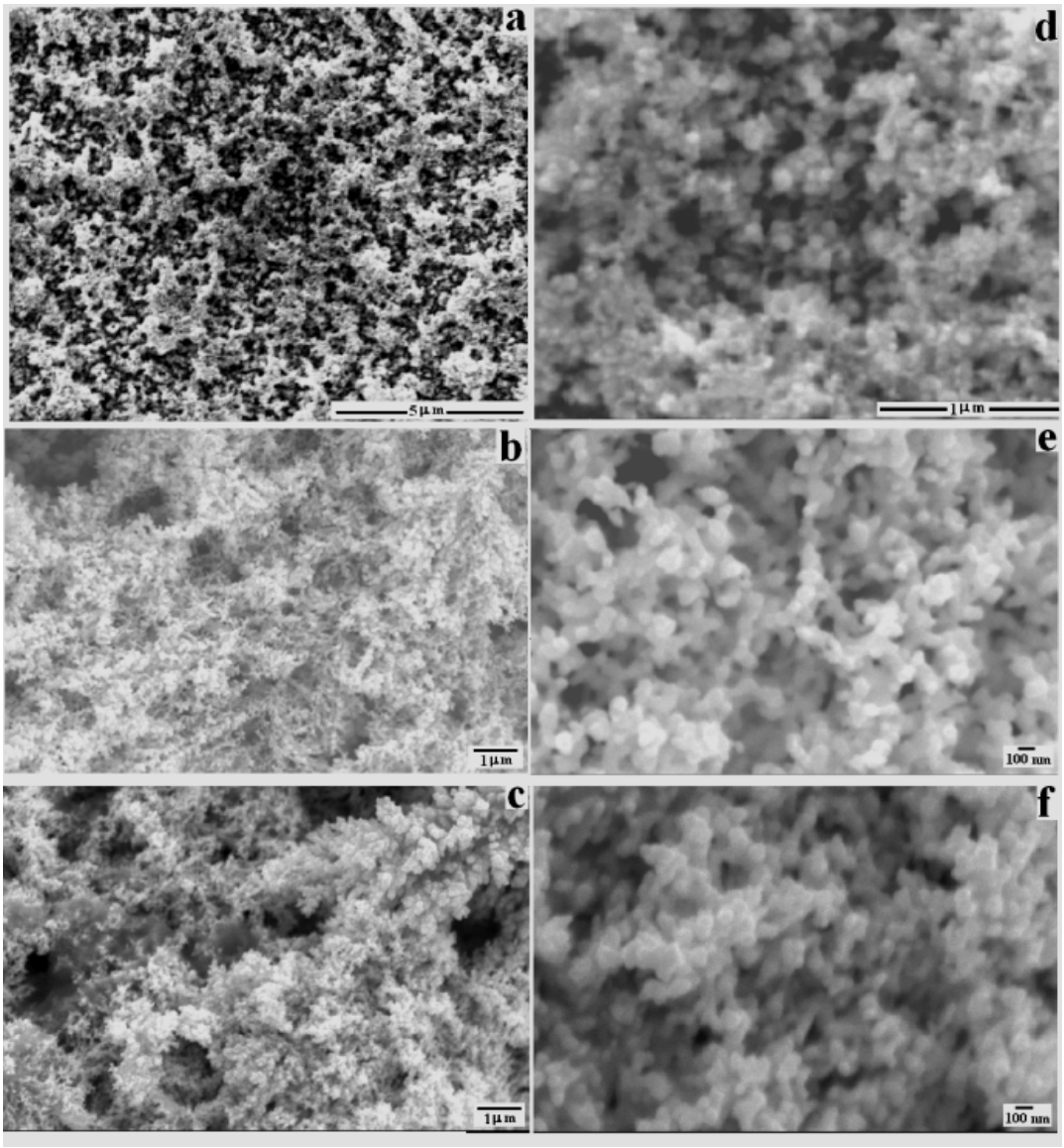

Figure 2. SEM images of electrochemically grown Au NP surface using MUA and KCl (a) 30, (b) 60 and (c) 90 minutes of deposition time and corresponding higher magnification images are (d), (e) and (f) respectively.

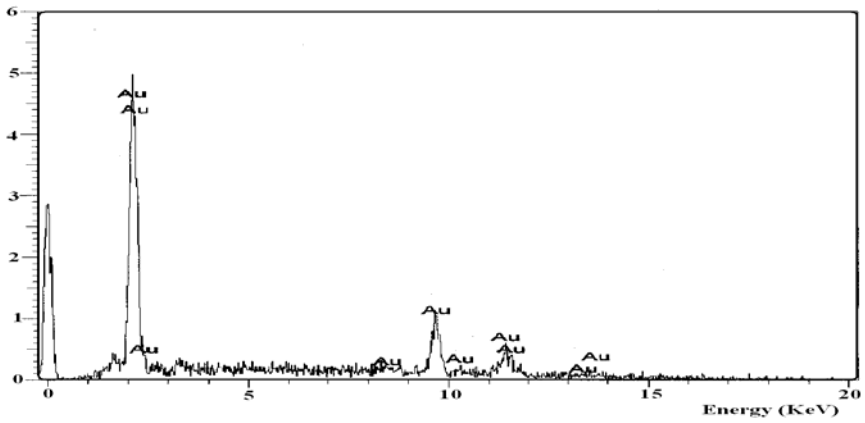

Figure 3. EDAX of electrochemically grown Au NPs for 30 minutes using MUA and KCl.

Element	% (weight)
O	3.19
Cl	0.83
K	1.45
Au	94.53

Table 1. Shows the EDAX results of electrochemically grown Au NPs grown surface using MUA and KCl.

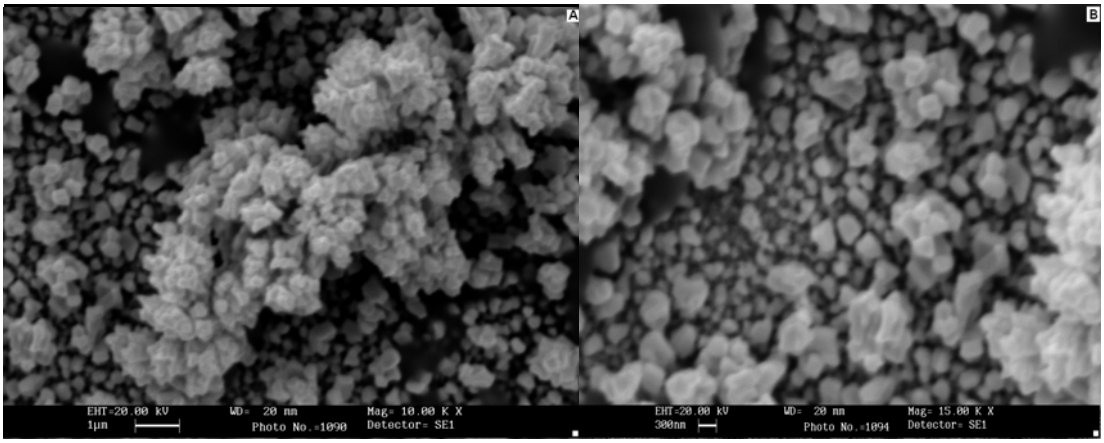

Figure 4. (a) SEM image of gold deposited for 30 minutes deposition time in equal volumes of KCl, MUA, and $NaBH_4$, (b) High resolution image of the same region.

3.3.2 AFM Studies

The AFM studies were carried out on the evaporated gold coated porous Au NPs film. Since the surface was very rough it was difficult to scan the surface at large scan ranges. However, it was possible to obtain good reproducible images at lower scan ranges. Figure 5 shows the 2 μm x 2 μm range tapping mode AFM image of the mesoporous gold surface. The image shows several vertically arranged columns that are irregularly distributed with voids separating them. The surface height as shown in the image extends to about 350 nm. The gaps that exist between the columns produce the observed porous structure which is seen in the SEM image of Figure 2a. The AFM image clearly reveals the very high roughness of the surface film, which is responsible for the observed large surface area.

3.3.3 Surface X-ray Diffraction (XRD) Studies

Surface X-ray diffraction measurements of Au NPs coated surface were carried out using Cu Kα radiation with a wavelength of 1.540 Å. The 2θ values were varied from 10^{o} to 90^{o}. Figure 6a shows the surface XRD of mesoporous gold. The broadened XRD peaks for the mesoporous gold surface compared to the sharper bulk gold XRD (Figure 6b) indicates the presence of nanometer sized particles on the mesoporous gold surface. It can be seen that the reflections from the Au NPs are same as that of bulk gold which are indexed to the face centered cubic (fcc) structure of Au. The size of the particle is calculated from full width at half maximum (FWHM) using Debye-Scherrer equation which is given by: $\chi_s = 0.9\,\lambda$ / FWHM cos θ Where χ_s is the crystalline size, λ is the wavelength of X-ray and θ the diffraction angle.

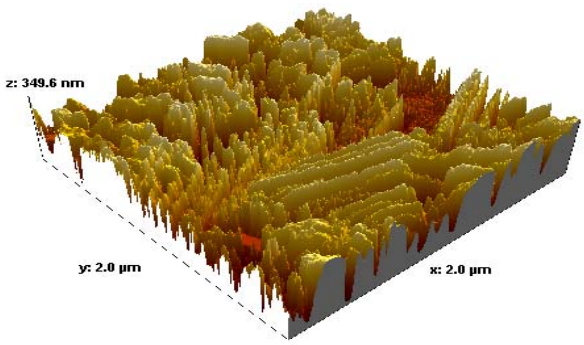

Figure 5. Shows the AFM image of the electrochemically grown Au NPs film using MUA and KCl.

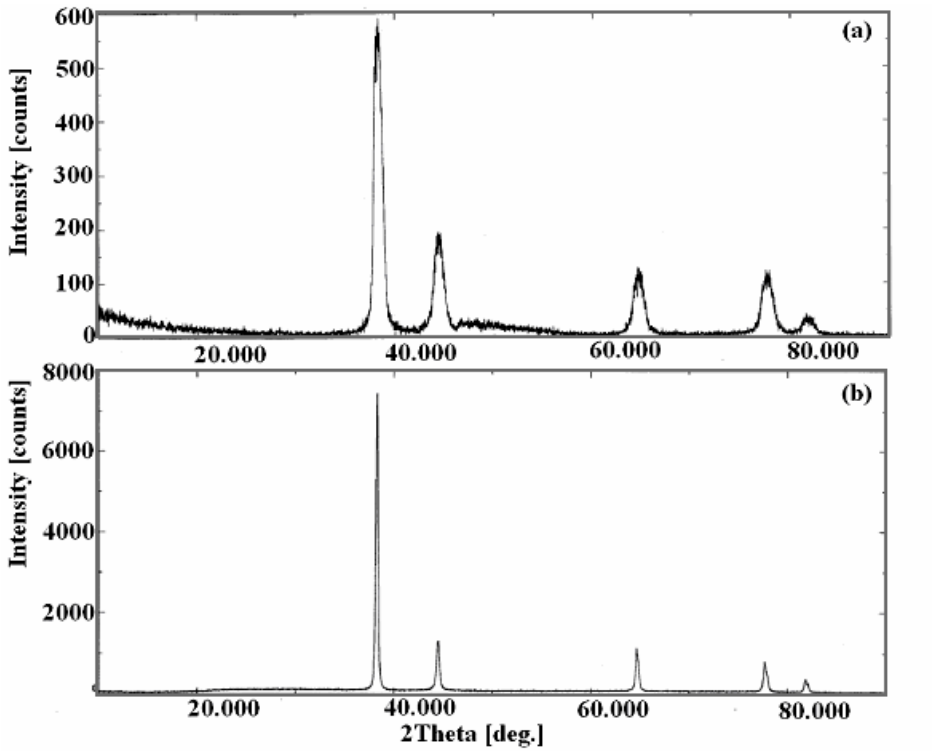

Figure 6. XRD of electrochemically grown mesoporous gold using MUA and KCl (a) and bulk polycrystalline gold substrate (b).

Table 2 summarizes the values of 2θ, indexing of plane, full width at half maximum (FWHM) and sizes of nanoparticles and bulk gold surfaces obtained from XRD. The nanoparticles size of 7.44 nm was calculated from the values for (111) plane, using Debye- Scherrer equation. The particle size of 32.6 nm was calculated from the values for (111) plane for bulk substrate electrode.

3.3.4 Mechanism of Formation

Normally, electrodeposition at high current density should produce dendrites or loose powdery coating as the current is far above the limiting current density for the electrodeposition process [14]. This indeed is observed when the electrodeposition is carried out in the absence of the thiol, MUA in the electrolyte where the deposit was gray in color, powdery and did not adhere to the electrode surface well and flaked off easily by tapping. In contrast, the deposit obtained in the presence of MUA is black, well adherent and can be subjected to extensive electrochemical experimental studies without any damage to the surface. This clearly establishes that the presence

of the thiol in the electrolyte is essential for the formation of well adherent mesoporous film of gold on the surface.

Surface	2θ	Indexing of planes	FWHM	d-value	Size (nm)
Bulk gold	38.300	(111)	0.259	2.3481	32.6
	44.500	(200)	0.235	2.0343	62.9
	64.680	(220)	0.141	1.4399	41.0
	77.700	(311)	0.235	1.2280	39.5
	81.840	(222)	0.235	1.1760	40.7
Au NPs	38.120	(111)	1.129	2.3588	7.4
	44.280	(200)	1.012	2.0439	8.4
	64.260	(220)	0.447	1.4483	21.2
	77.120	(311)	0.306	1.2357	33.2
	82.000	(222)	-------	1.1741	-------

Table 2. XRD data for mesoporous gold surface and bulk gold surface and the particle sizes for different planes

It is known that in the case of synthesis of Pd nanoparticles, the charged species, Pd_n^{m+} is formed at the anode, which migrate and discharge at the cathode to form Pd^0 clusters that are subsequently associated and stabilized by tetraalkylammonium salts in the solution [15]. Similarly, in the present case, we propose the following mechanism for the formation of the mesoporous gold on the surface. The gold electrode had been earlier shown to dissolve as monovalent $[AuCl_2]^-$ and predominantly as trivalent $[AuCl_4]^-$ complexes during the dissolution in the aqueous chloride solution [16]. It is well known that $[AuCl_2]^-$ forms polymeric thiolated complex in the presence of organic thiol, which acts as a chelating ligand [17-19]. In this case, the ethanol in the solution reduces the trivalent complex $[AuCl_4]^-$ to monovalent complex $[AuCl_2]^-$. This monovalent complex forms the polymeric thiolated complex $(Au^+(SR))_n$ with MUA, where R represents the undeconic acid chain which subsequently reaches the cathode electrophoretically and is reduced in

the form of gold nanoparticles on the surface. At the high current density, well above the limiting current density, the deposition takes place by fresh nucleation in different sites, creating new grains instead of the normal layer type growth preferred at low current densities [14]. The thiolated polymer complex is also reduced by ethanol and forms gold nanoparticle in the solution as evidenced by its color and the UV-vis spectra of the extracted gold nanoparticles in the solution [13].

3.3.5 Electrochemically Active Surface Area of Mesoporous Gold on Gold

The electroactive surface area (true surface area) of the porous Au deposit is of primary importance in electrocatalysis and supercapacitor applications. We determined the true surface area by cyclic voltammetry in 0.1 M $HClO_4$ by measuring the charge associated with the cathodic Au oxide stripping peak. Figure 7 shows the cyclic voltammograms in 0.1 M $HClO_4$ for a gold disc electrode and the electrode deposited with Au nanoparticles for different time durations. The voltammograms exhibit the typical behavior of polycrystalline Au in acid electrolyte with a clear Au oxide-stripping peak during the cathodic cycle. The real surface area of gold nanoparticles coated surface can be estimated from the amount of charge consumed during the reduction of Au surface oxide monolayer and the reported value of 390 μC cm^{-2} for the process [20]. The electroactive surface areas for the Au disc electrodes (of geometric area of 0.002 cm^2) are thereby measured to be 0.9 cm^2 for 30 minutes deposition time. Table 3 summarizes the roughness factor, true surface area results for Au NPs surface at different deposition time and bulk gold electrode surface. The disproportionately large increase after 90 minutes of deposition is due to the extended growth of the film laterally around the disc over the polished face of the glass surface used for sealing the gold wire. This overgrowth was intact and could not be removed by simple water jet cleaning used for rinsing or by electrochemical potential cycling. Further work on this may provide a simple route for preparing freestanding gold nanoparticles films. Table 4 shows the true surface area obtained for the electrodes prepared at different current densities. While the measured true surface area increases, as expected with the current density, the value plateaus after 0. 4 A cm^{-2}. The deposition of Au NPs was carried out at different thiol concentration. The true surface area measured for Au NPs surfaces deposited at different thiol concentration are shown in the Table 5. With increasing thiol concentration, surface area increases up to 15 mM. The surface area decreases with further increase in the thiol concentration. The deposition of Au NPs at different

ratio of water to ethanol such as 1:1, 2:1, 3:1, and 4:1 respectively, was carried and measured the true surface area. The results are shown in table 6. The measured true surface area decreases with decrease in ethanol concentration. This shows that, ethanol as a reducing agent plays a major role in Au NP formation.

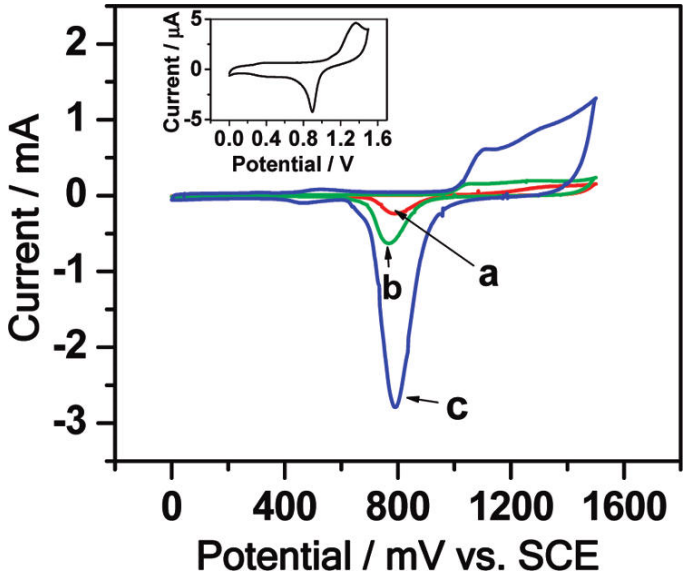

Figure 7. Cyclic voltammograms at a scan rate of 100 mV s^{-1} recorded in 0.1 M $HClO_4$ for mesoporous gold deposited for (a) 30 minutes, (b) 60 minutes. (c) 90 minutes using MUA and KCl. Inset shows the CV for bare gold electrode in the same electrolyte. (Electrode geometric area = 0.002 cm^2)

Figure	Deposition time	Q (µC)	Roughness factor	True surface area (cm^2)
7(a)	30 minutes	366.6	458.2	0.9164
7(b)	60 minutes	873.1	1091.3	2.182
7(c)	90 minutes	3907	4883.7	9.767
7(Inset)	----------	3.869	4.8	0.0096

Table 3. Summary of deposition time and total surface area of gold nanoparticles and bulk gold surfaces.

Current density (A/cm^2)	Q (µC)	True surface area (cm^2)
0.1	71	0.18
0.2	142	0.36
0.3	177	0.45
0.4	422	1.08
0.5	366	0.93

Table 4. The measured charge and the electroactive true surface area obtained from the gold oxide stripping current in 0.1M $HClO_4$ for 30 minutes of mesoporous gold deposition at different current densities on the gold disc electrode of geometric area 0.002 cm^2.

Thiol Concentration (mM)	Q (µC)	True surface area (cm^2)
5	279	0.7
10	366	0.93
15	490	1.25
20	334	0.85

Table 5. Shows the stripping results of Au NP coated surface for different thiol concentration for 30 minutes of deposition.

Ratio of water and ethanol	Q (μC)	True surface area (cm^2)
1:1	366	0.93
2:1	237	0.60
3:1	220	0.56
4:1	135	0.34

Table 6. Shows the stripping results of Au NP coated surface for different water and ethanol ratio for 30 minutes of deposition.

3.4 Electrochemical Features of Au NP Modified Electrodes for Redox Probes

As described earlier the mesoporous gold nanoparticles (Au NPs), which are formed *in situ* as a film onto the gold surface shows very high real surface area. The Au NPs film also exhibits interesting electrochemical properties. We have studied the electrochemical properties of the mesoporous Au NP deposit using cyclic voltammetry (CV). The electron transfer properties of redox probes such as potassium ferrocyanide, $K_4[Fe(CN)_6]$ and hexamineruthenium (III) chloride, $[Ru(NH_3)_6]Cl_3$ show deviation of Randles-Sevcik equation at higher scan rates in cyclic voltammetry. This is due to the different diffusional behavior of redox probes at the bulk gold and Au NP electrode surfaces as shown by Compton *et al.* for adsorbed nanoparticles [22].

3.4.1 Cyclic Voltammetry Studies

Cyclic voltammetry is an important technique to study the electron transfer reactions of the redox probes at surfaces. It was reported that the mercaptoundecanoic acid functionalized Au NPs adsorbed onto the graphite surface by simple immersion process shows an enhanced current in cyclic voltammetry in $K_4[Fe(CN)_6]$ compared to the bare graphite electrodes [21]. We have studied the electrochemical features of the *insitu* deposited Au NP electrodes using standard redox probes, $K_4[Fe(CN)_6]$ and $[Ru(NH_3)_6]Cl_3$. Figure 8a shows the cyclic voltammograms of bulk gold in $K_4[Fe(CN)_6]$ at different scan rates. Figure 8b shows the corresponding I verses $\nu^{1/2}$ plots. The I vs $\nu^{1/2}$ plot is linear for bulk gold electrode and follows Randles-Sevcik equation. Figure 9a shows the CVs at different scan rates for Au NP electrode in $K_4[Fe(CN)_6]$ and the

corresponding I verses $\nu^{1/2}$ is shown in the Figure 9b. The Au NP electrode of same geometric area (0.002 cm^2) in this case shows enhanced currents compared to the bulk gold electrode and plot of I vs $\nu^{1/2}$ deviates from linearity, especially at higher scan rates.

Compton et. al. developed a theory for the diffusional current at nanoparticles-modified electrodes for different surface coverage of NPs and showed that the electrocatalytic reduction of protons at NP electrode corresponds to the theory [22]. For very high surface coverage of NPs, I vs $\nu^{1/2}$ is linear. For low surface coverage of NPs, plots of I verses $\nu^{1/2}$ shows the deviation from the linearity at higher scan rates. This phenomenon explained based on the diffusional characteristics. For very low surface coverage of the particles, where there is no overlap of neighboring diffusion zones, the plot of I vs $\nu^{1/2}$ is not linear. This is due to the spherical diffusion of ions to the surface. However, for high surface coverage of particles, diffusional behavior occurs with extreme overlapping of neighbouring diffusion zones. This overlap of diffusion fields leads to shielding of the electroactive species diffusing towards the surface. Due to this shielding of the diffusion, mass transport decreases. In this case, the plot of I vs $\nu^{1/2}$ is linear. This type of diffusion is similar to the planar diffusion of ions to the surface.

In our case the plot of I verses $\nu^{1/2}$ deviates from linearity, especially at higher scan rates, showing that the diffusion zones do not overlap for the electro active species. Under these diffusional regime, these particles are able to draw a higher current because of their height above the electrode surface which makes them diffusionally accessible to a greater region of the solution on a short experimental time scale. Hence, especially at higher scan rates the I verses $\nu^{1/2}$ plots deviates from linearity. In the present studies although the surface coverage is very high as shown in the Figure 2b of SEM image, the majority of the particles are well separated from each other. This mimics the individual nanoparticles for diffusion of the species. These NPs can draw higher current due to greater diffusional accessible surface area for the redox species. Hence, the I vs $\nu^{1/2}$ shows deviation from the linearity. This as explained earlier is due to the spherical diffusion of ions to the surface [22].

Figure 10 shows the schematic representation of diffusion of ions to the different surfaces. As can be seen that diffusion at single particle is spherical, where as the overlap diffusion takes place with increasing density of particles leading to a planar diffusion. Figure 11 shows the diffusion of ions to the surface having different density of particles. This shows that at small time scales, spherical diffusion takes place and at longer time scales hemispherical

diffusion takes place. If the particles are very close, these diffusion domains overlap especially at longer time scales.

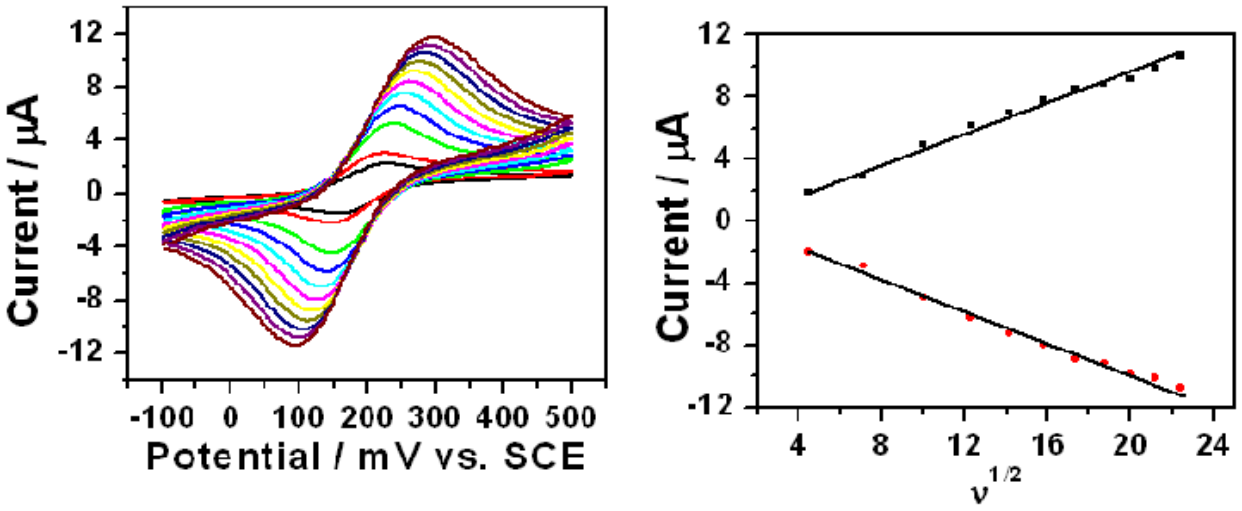

Figure 8. (a) CVs of bulk gold electrode at different scan rates in 10 mM $K_4[Fe(CN)_6]$ and (b) plot of I vs. √ν.

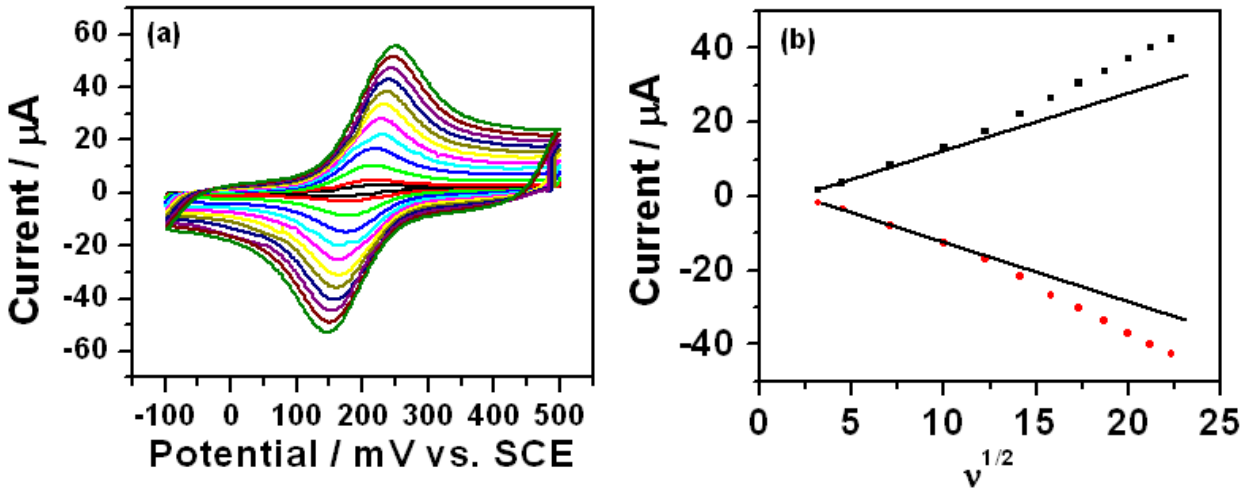

Figure 9. (a) CVs of electrochemically grown Au NPs using MUA and KCl electrode at different scan rates in 10 mM $K_4[Fe(CN)_6]$ and 1M NaF, (b) plot of I vs. √ν

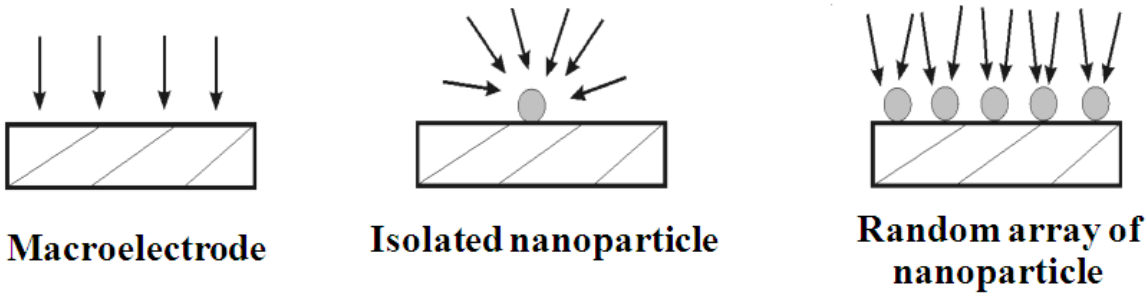

Figure 10. Shows schematic representation of diffusion pattern of species to the different type of surfaces

We have also studied the redox properties of $[Ru(NH_3)_6]Cl_3$ at bulk and Au NP electrodes. Figure 12a-b show the I verses $v^{1/2}$ plots for the bulk gold and Au NP electrodes. The Au NP electrode shows the enhanced currents compared to the bulk gold electrode. It shows that the I verses $v^{1/2}$ is linear for bulk gold electrode and non-linear for Au NP electrode at the scan rates studied. The non-linearity of Au NP electrode in $[Ru(NH_3)_6]Cl_3$ at higher scan rates is similar to the behavior of the Au NP electrode in $K_4[Fe(CN)_6]$.

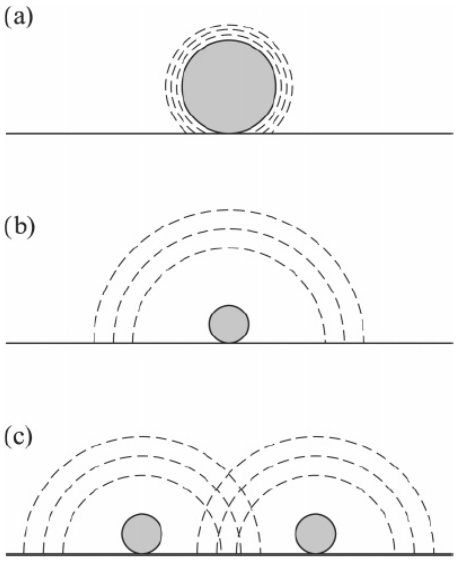

Figure 11. Shows the diffusion of species to the surface (a) small time scales (spherical), (b) longer time scales (hemi spherical), and (c) Overlapping diffusion domain at longer time scales [22].

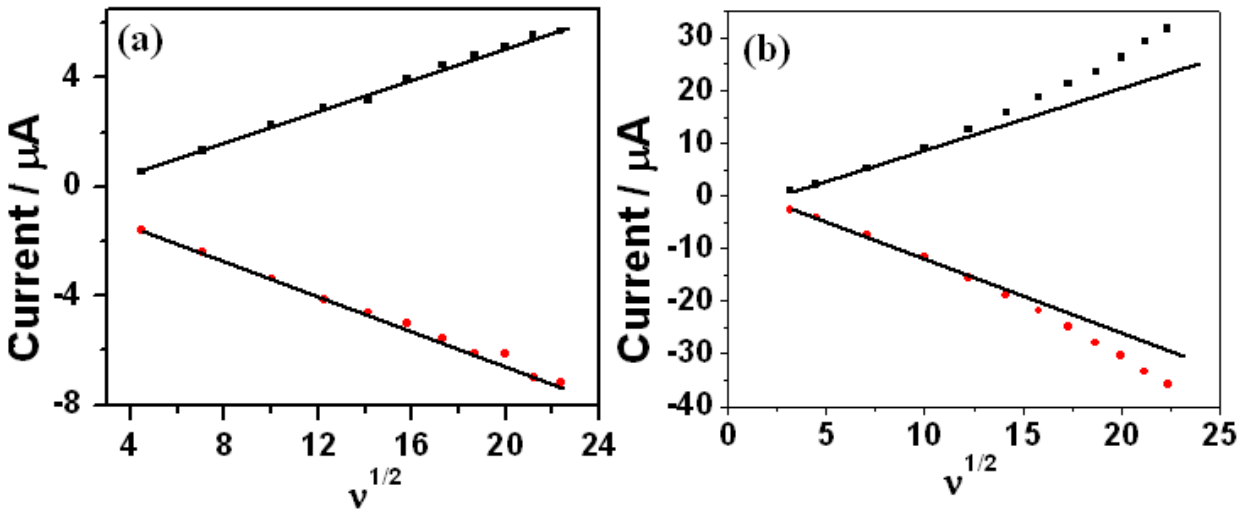

Figure 12. I vs. √ν plots of (a) Bulk gold electrode and (b) Electrochemically grown Au NPs using MUA and KCl electrode in 5mM $[Ru(NH_3)_6]Cl_3$ and 1M KCl.

3.5 Mesoporous Au NP Electrode for Dopamine Detection at Neutral pH

Dopamine is one of the most important neurotransmitters and it plays a very crucial role in the function of the central nervous, hormonal, and cardiovascular systems. It is widely admitted that a major problem encountered with the electrochemical detection of DA is the interference of ascorbic acid (AA), which largely coexists with DA in brain tissue. Both of them have an overlapping oxidation potential on the solid surfaces [24].

As the concentration of AA in the biological samples is relatively higher than that of DA, the selectivity and sensitivity are of equal importance in the fabrication of the voltammetric sensor. The direct oxidation of DA at the bulk electrodes occurs at a potential close to that of AA and very often the bulk electrodes suffer from fouling by the oxidation products, which results in poor selectivity and reproducibility. Recently, Au nanoparticles have been widely used for the voltammetric sensing of DA in the presence of AA [25-29].

We have studied the electrochemical oxidation of DA and interference effects from AA at the bulk gold and Au NP electrode in aqueous phosphate buffer solution (pH 7) using CV and square wave voltammograms (SWV).

3.5.1 Cyclic Voltammetry Studies

Figure 15 shows the CVs of bulk gold and Au NP electrode in the absence and presence of 84 x 10^{-6} M DA solution in phosphate buffer solution of pH 7.0 at a scan rate of 100 mV/s. Au NP electrode exhibits enhanced electrocatalytic oxidation current of DA when compared to the bulk gold electrode. The enhanced catalytic oxidation current of DA at the Au NP electrode is due to the higher surface area and also spherical diffusion of DA to the NPs modified surface, which increases the mass transport to the surface.

Figure 16 shows the I verses $\nu^{1/2}$ plots for the bulk gold and Au NP electrode in dopamine solution. It can be seen that I verses $\nu^{1/2}$ plots are linear in case of bulk gold electrode, where as it is non-linear, especially at high scan rates in the case of Au NP electrode for the oxidation of DA. This non-linearity is due to the different diffusional behavior for DA at Au NP electrode, which is similar to the behavior of $K_4[Fe(CN)_6]$ and $[Ru(NH_3)_6]^{3+/2+}$ at Au NP electrode discussed earlier. At the Au NPs electrode, spherical diffusion of DA takes place especially at higher scan rates.

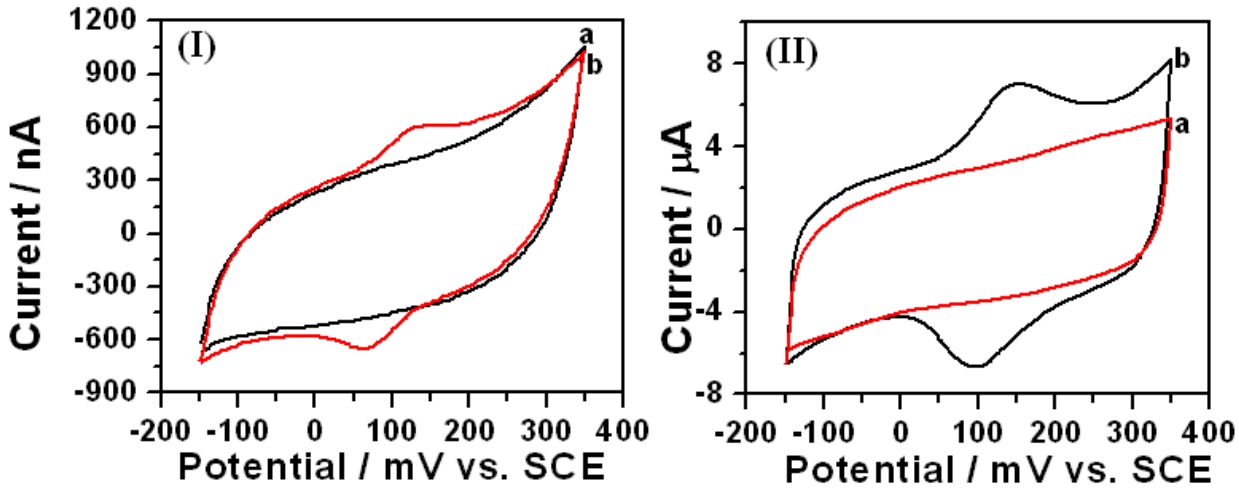

Figure 15. (I) CVs of bulk gold electrode in the absence (a) and presence (b) of 84 µM DA at a scan rate of 100 mV/s. (II) CVs of electrochemically grown Au NPs using MUA and KCl electrode in absence (a) and presence (b) of 84 µM DA at a scan rate of 100 mV/s.

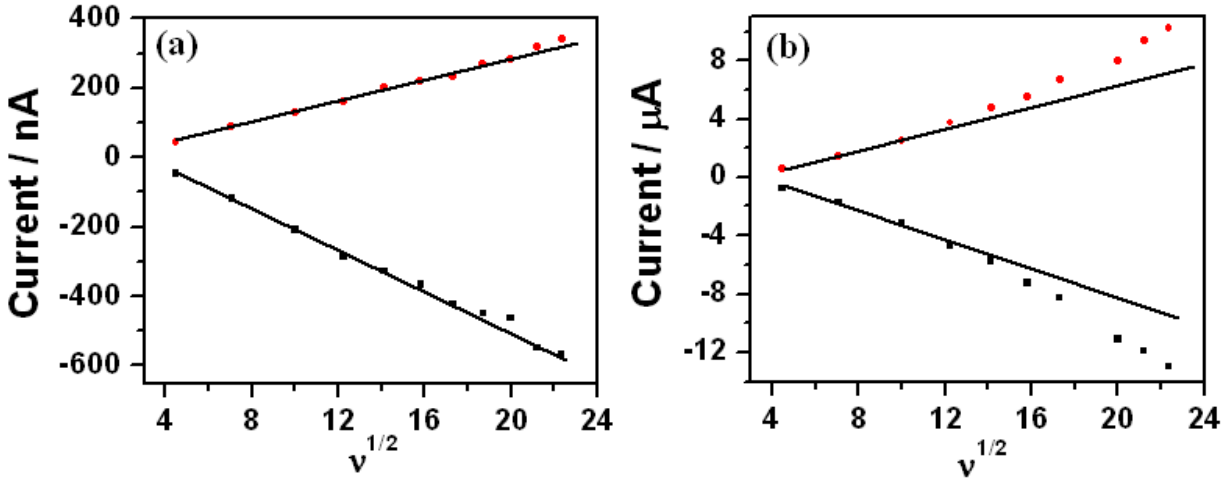

Figure 16. Plots of I vs. √ν in dopamine solution for (a) Bulk gold electrode and (b) Au NP electrode.

3.5.2 Square Wave Voltammogram (SWV) Studies

Figure 17a shows the SWV curves for different concentration of DA solution. The concentration of DA was increased in steps of 21 µM. With increasing concentration of DA, current increases. The Figure 17b is the calibration plot for the DA detection. It is almost linear in the concentration range of 21 to 147 µM. The detection limits for the bulk gold and Au NP electrode were found to be 50 x 10^{-6} M and 20 x 10^{-7} M respectively.

Selectivity of Au NP electrode for determination of DA was evaluated in the presence of high concentration of AA at the bulk gold and Au NP electrode. Figure 18 shows the SWVs recorded for a mixture of AA (1 x 10^{-4} M) and DA (147 x10 $^{-6}$ M) at the bulk gold (figure 18a) and Au NP (figure 18b) electrode in phosphate buffer. A current response with a overlapped peak was observed for the oxidation of AA and DA at the bulk gold electrode. Bulk gold electrode could not effectively discriminate the voltammetric signals from AA and DA. On the other hand, two well-separated voltammogram were observed for the oxidation of AA and DA, at the Au NP electrode. The well separated peaks for dopamine and ascorbic acid in the case of mesoporous gold surface may be due to the difference in the diffusion mechanism compared to the planar bulk gold surface. The higher rate of mass transport due to spherical diffusion process in the case of mesoporous Au surface can contribute to separation in the current profiles of dopamine and ascorbic acid as seen in Figure 18(b).

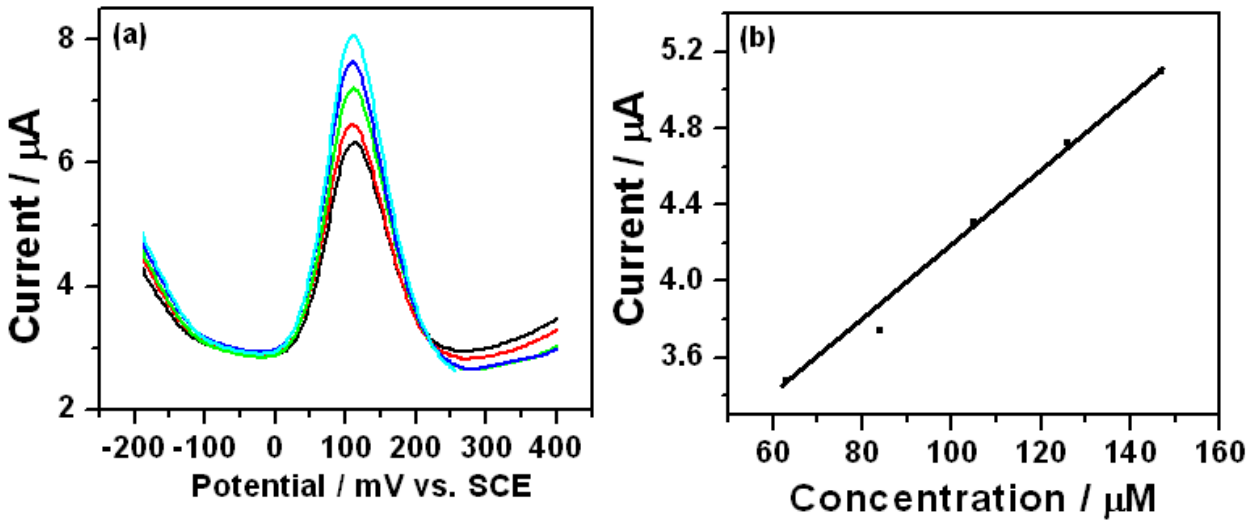

Figure 17 (a) Square wave voltammograms of electrochemically grown Au NPs electrode in different concentration of DA and (b) Calibration plot

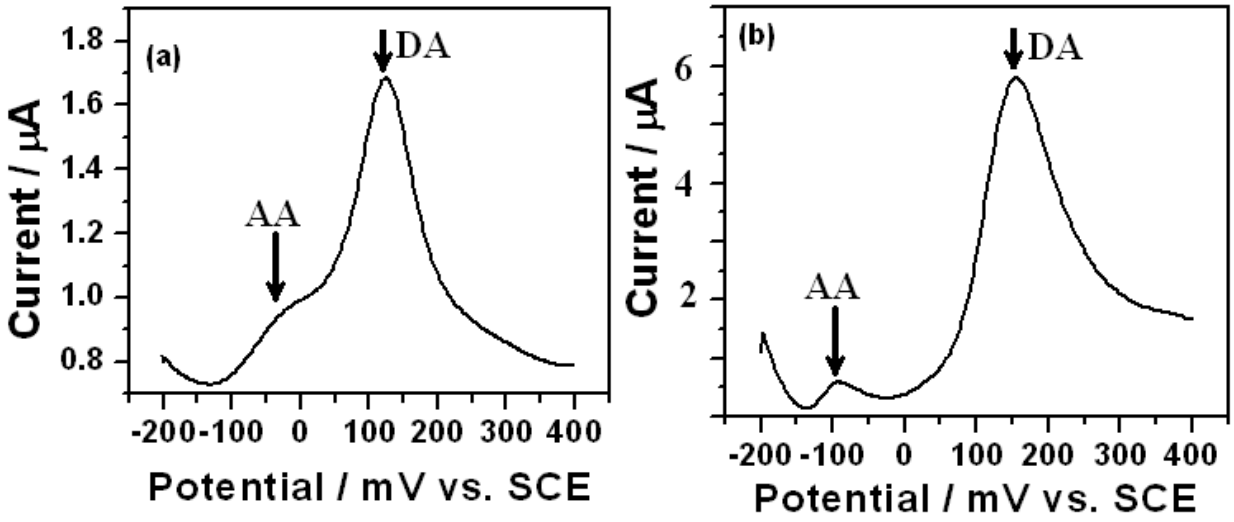

Figure 18. Square wave voltammograms in the mixture of 147 x10 $^{-6}$ M DA and 1 x 10^{-4} M AA. (a) Bulk gold electrode and (b) Electrochemically grown Au NPs electrode.

3.6 Mesoporous Au NP electrode as a Hydrogen Evolution Reaction (HER) Catalyst

The HER has been studied in literature using polycrystalline and single crystal gold electrode [30-35]. In the present work we have used the mesoporous gold electrode to show its potential as hydrogen evolution catalyst.

3.6.1 Cyclic Voltammetry Studies

We have studied the HER in 0.1M $HClO_4$ using CV and chronoamperometry under N_2 atmosphere. Figure 21 shows the CVs of bulk gold and Au NP electrode. It can be seen that the currents due to HER at Au NP coated electrode is very much higher than the bulk gold electrode. The hydrogen evolution starts at much less negative potential of (-0.4 V) compared to that in bulk gold. The very high hydrogen evolution current and lower overpotential for the hydrogen evolution points to increased catalytic activity of Au NPs coated electrode.

Figure 22 shows the Tafel plots, which are determined from the chronoamperometry. We find that the slope of the Tafel plot is 0.105 V for bulk gold electrode, which is in the range of -0027 V to -0.15 V reported for polycrystalline electrodes. The slopes for the Au NP electrode was found to be 0.059 V, which is similar to Tafel slope reported for single crystal gold (111) electrodes.

The possible mechanism for the HER on electrode surfaces in acid solutions follows the steps [14, 36]:

$$H_3O^+ + M(e\text{-}) \longrightarrow MH_{ads} + H_2O \qquad (1)$$

$$2MH_{ads} \longrightarrow 2M + H_2 \qquad (2)$$

$$H_3O^+ + MH_{ads} + M\,(e\text{-}) \longrightarrow 2M + H_2O + H_2 \qquad (3)$$

Where, M represents a metal atom of the electrode, MH_{ads} is an adsorbed hydrogen atom on the metal surface, k_d (eq 1), k_c (eq 2), and k_{ed} (eq 3) are the rate constants of the discharge, chemical-desorption, and electrodic-desorption steps, respectively. Two basic reaction paths of the HER are regarded as likely: a primary discharge step (eq 1) followed by either chemical-desorption (eq 2) or electrodic-desorption (eq 3). These two pathways are termed as the Volmer-Tafel and Volmer-Heyrovsky mechanisms, respectively. If discharge is the rate-determining step (RDS), the amount of adsorbed hydrogen on the metal surface tends to be low since the adsorbed hydrogen atoms generated in this step react and are desorbed swiftly. If desorption is the RDS, hydrogen atoms accumulate at the surface. In the present case for Au NP, the Tafel slope of 59.86 mV, which is very close to 2.3 RT/F (60 mV) obtained for the HER. This value of slope indicates that the primary discharge step is constrained to be almost at equilibrium. Usually this happens because the desorption step in equation (eq 2) is rate controlling [32].

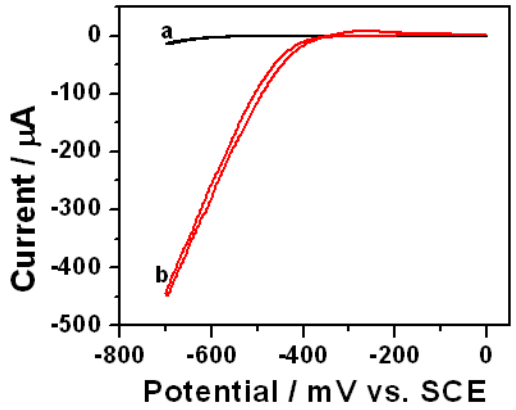

Figure 21. CVs of (a) bulk gold electrode and (b) Au NP electrode in 0.1 M $HClO_4$ under N_2 atmosphere.

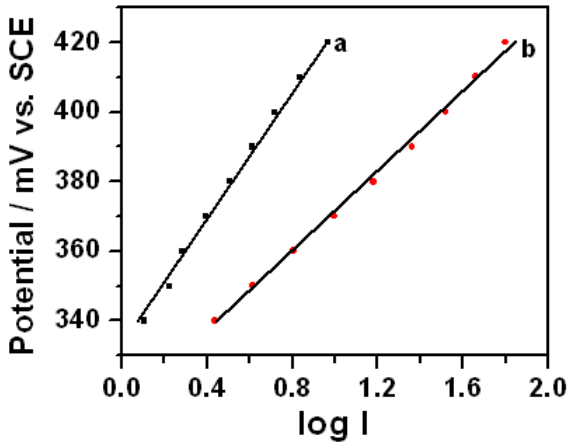

Figure 22. Tafel plots of (a) bulk gold electrode and (b) Au NP electrode in 0.1 M $HClO_4$ under N_2 atmosphere.

3.7 Electrochemical Double Layer Capacitance Measurements of Porous Au NP Modified Electrode Surfaces

The porous metal coatings find potential applications in electrochemical capacitors and sensors. The high surface area porous Au in our studies showed high roughness factor a value of about 4883.7, making it a potential candidate for supercapacitor applications. The double layer capacitance of porous Au has been evaluated electrochemically in 0.1 M $HClO_4$ and 1M KOH solution. For porous electrode, CV is one of the important techniques for evaluating the capacitive behavior of any material. Figure 24 shows the cyclic voltammograms of Au NP

deposited surfaces in acid and alkaline medium. A rectangular shaped voltammogram with a large current separation and symmetric in both cathodic and anodic directions are the indicators of an ideal capacitor. The capacitive values are determined by measuring the integrated charge from CV.

Figure 25 shows the capacitance versus scan rate plots for three different deposition times. It can be seen that the capacitance values increase with increasing time of deposition. This reflects an increase in the surface area with deposition time. The measured capacitance is the highest at the lowest scan rate of 2 mV/s and decreases with increase in scan rate up to 10 mV/s as seen in the Figures 25(I) and 25(II). The capacitance values remains almost constant beyond a scan rate of 20 mV/s. Such a behavior reflects a high relaxation time for the double layer charging of the porous film. The highest capacitance values of 80 and 54.5 mF cm^{-2}, were obtained for 90 minutes deposition of Au NPs in 0.1 $HClO_4$ and 1M KOH respectively. This translates into about 35 F/g and 23 F/g of the coated film material. The capacitance values are higher in 1M KOH compared to that in 0.1M $HClO_4$ especially for 30 minutes of deposition time. The capacitance values are almost same both in acid and basic medium at higher scan rates for a particular time of deposition. Though gold as a supercapacitor material has not been explored in literature, due to it high cost it may find some specialized applications such as in microelectronics. Here, we have shown that the porous gold exhibits very high capacitance, though for a small range of potential in acid and alkaline medium. A more detailed study involving charge-discharge curves is required to totally explore its potential for application as a supercapacitor which is however, beyond the scope of the present thesis.

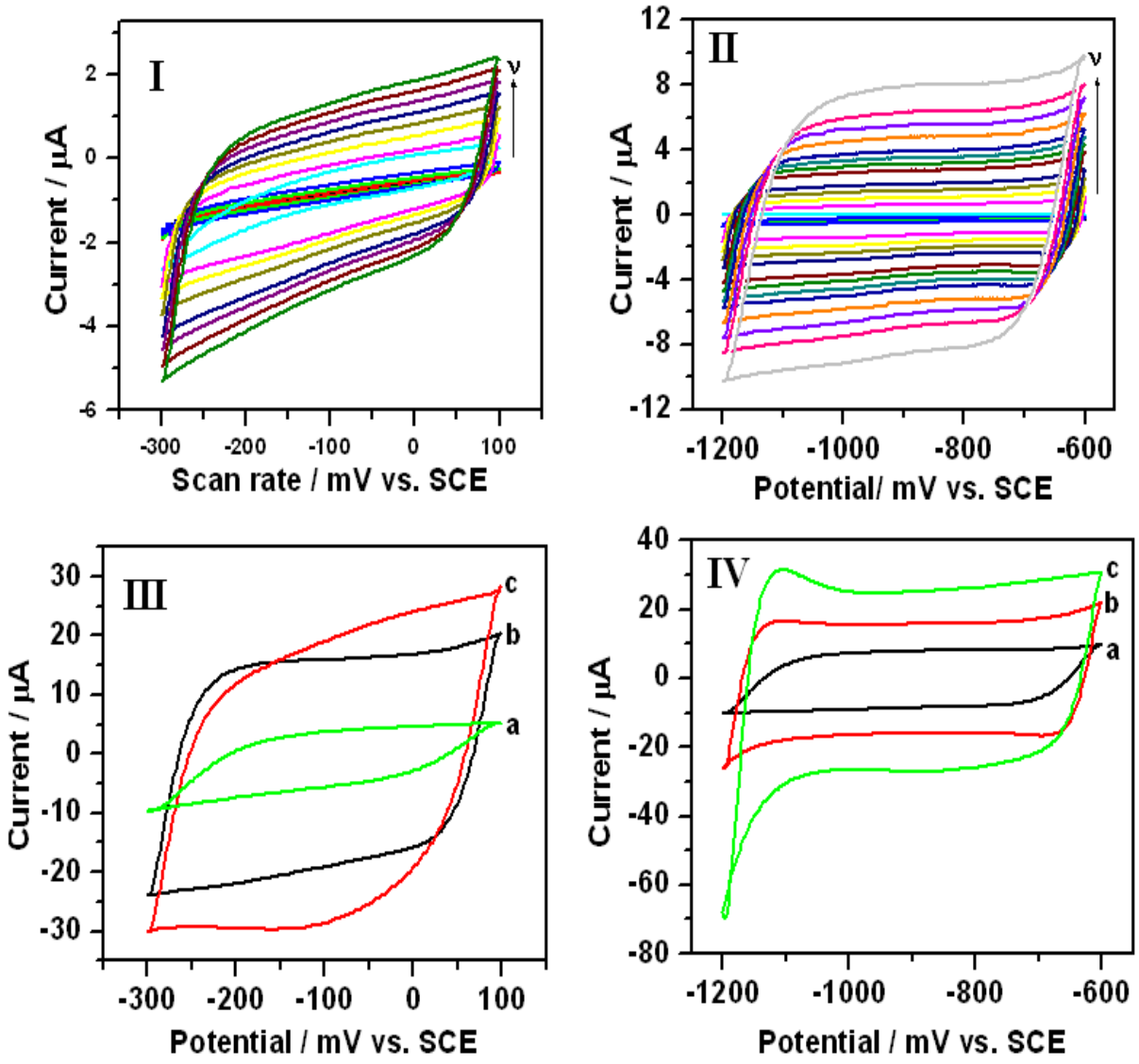

Figure 24. CVs of Au NP modified surface (I) 30 minutes deposited surface in 0.1M $HClO_4$ at scan rate of 2, 5, 10, 20, 50, 100, 150, 200, 250, 300, 350, 400, 450 and 500 mV s^{-1}, (II) 30 minutes deposited surface in 1M KOH at different scan rates similar to the figure 10(I), (III) For different deposition time in 0.1M $HClO_4$ at a scan rate of 500 mV s^{-1}: (a) 30 minutes (b) 60 minutes and (c) 90 minutes, and (IV) For different deposition time in 1M KOH at a scan rate of 500 mV s^{-1}: (a) 30 minutes (b) 60 minutes and (c) 90 minutes.

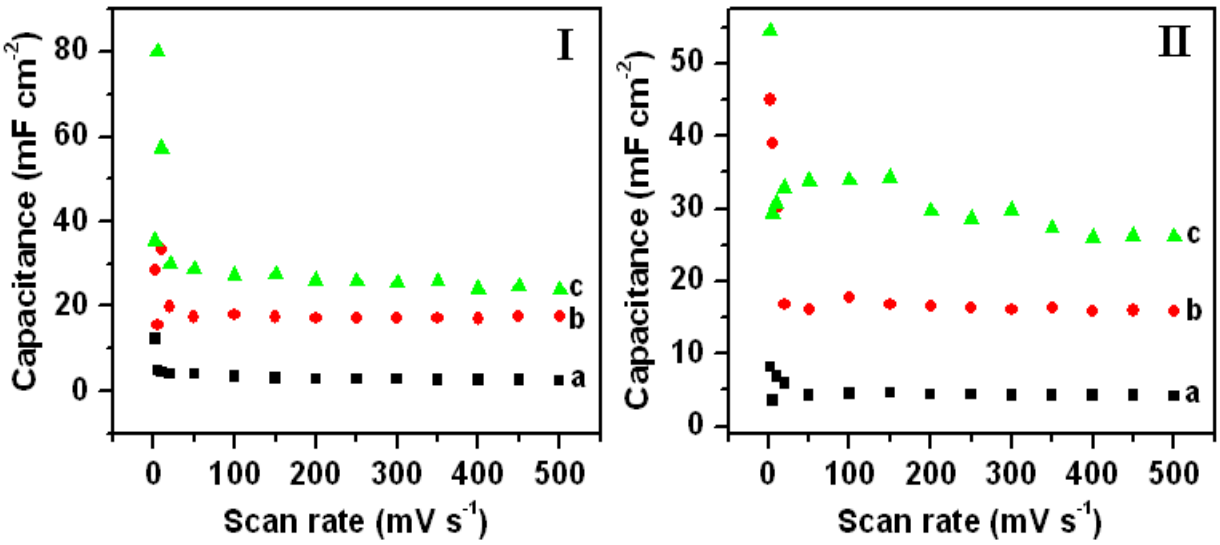

Figure 25. Capacitance versus scan rate plots of NP modified surfaces (I) acid medium: I(a) 30 minutes I(b) 60 minutes and I(c) 90 minutes of deposition and (II) alkaline medium: II(a) 30 minutes II(b) 60 minutes and II(c) 90 minutes of deposition.

3.8 Electrochemical Growth of Mesoporous Au NPs Film on Au using Decanethiol for Electro-Oxidation of Glucose

3.8.1 SEM Studies

The mesoporous gold electrodes described earlier used MUA in the electrolytic mixture. In the present section the mesoporous gold film was prepared in 20 mM decanethiol in ethanol and 1M KCl solution and was evaluated for glucose detection.

Figure 26a is the SEM image showing the porous structure of Au NPs film on gold surface. Figure 26b is the high resolution image of deposited gold which shows the individual nanoparticles of sizes about 10-25 nm. Figure 27 is the EDAX of Au NPs. EDAX results shows the 84.43 wt % of gold is present on the surface. In addition, surface has electrolyte component of 6.73 and 8.84 wt % Cl^- and K^+ respectively

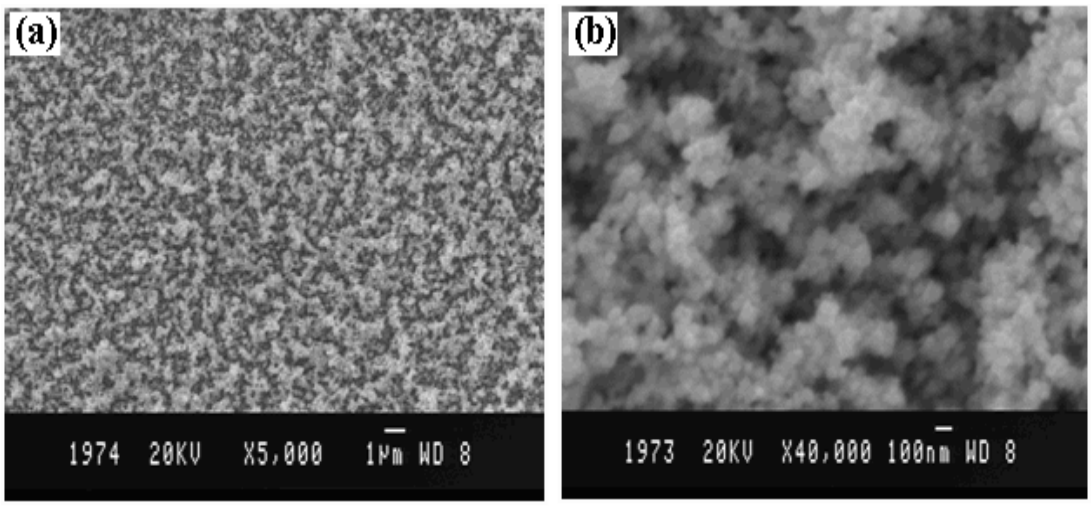

Figure 26. (a) SEM image of gold deposited in the presence of decanethiol, and KCl at a current density of 0.5 A cm^{-2} (b) High resolution image shows the individual nanoparticles.

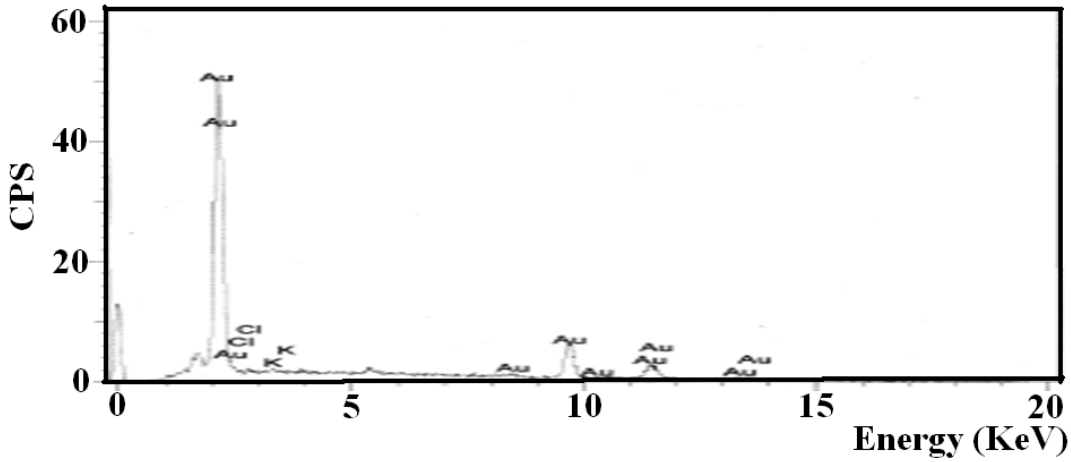

Figure 27. EDAX of Au NPs grown electrochemically in presence of DT and KCl for 30 minutes.

3.8.2 Electrochemically Determined Active Surface Area

We have determined the electroactive surface area by cyclic voltammetry in 0.1 M $HClO_4$ by measuring the charge associated with the cathodic Au oxide stripping peak. Figure 28 shows the cyclic voltammograms in 0.1 M $HClO_4$ for Au NPs electrode deposited for 30 minutes duration. The voltammogram exhibit the typical behavior of polycrystalline Au in acid electrolyte with a clear Au oxide-stripping peak during the cathodic cycle. The real surface area of gold nanoparticles coated surface can be estimated from the amount of charge consumed during the reduction of Au surface oxide monolayer and the reported value of 390 μC cm^{-2} for the process [20]. The charge associated with stripping is measured to be 166 μC. The electroactive surface area for the Au disc electrodes (of geometric area of 0.002 cm $^{2)}$ is thereby estimated to be 0.42 cm^2 for 30 minutes deposition time.

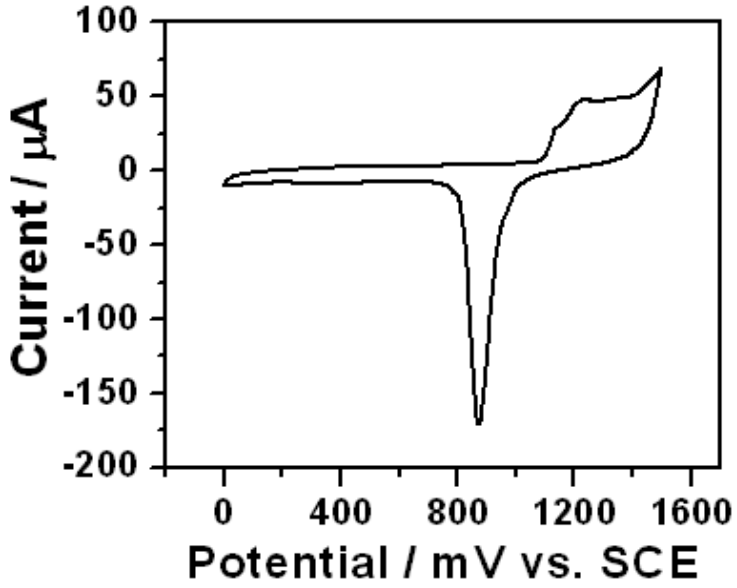

Figure 28. Cyclic voltammogram at a scan rate of 100 mV s^{-1} recorded in 0.1 M $HClO_4$ for Au NPs grown electrochemically in presence of DT and KCl.

3.8.3 Glucose Detection

To obtain highly reliable and fast monitoring of blood sugar for the treatment and control of diabetes, the development of amperometric glucose sensors has been a challenge [37-38]. Most of the studies to develop the reliable and fast monitoring device have involved the use of the enzyme glucose oxidase, which catalyzes the oxidation of glucose to gluconolactone. In these

devices, the enzyme is contacted by a redox mediator, which is reduced by the enzyme and reoxidized at the surface of an electrode. Mediators also used to access the flavin cofactor of glucose oxidase electrochemically [39]. In addition to these, oxygen consumption can be used as an indicator in glucose sensor where, oxygen is reduced by the enzyme to hydrogen peroxide, which is oxidized at an electrode surface. However, the lack of stability due to the intrinsic nature of enzymes remains the main problem in the practical application of such sensors [40-42]. Therefore, numerous studies have been devoted to the investigation and preparation of glucose sensors without using enzymes [40, 43-45]. In some studies, the use of bare platinum or gold electrodes was proposed [46-49]. However, these electrodes suffer from low sensitivity, poor selectivity and poisoning by intermediates and chloride [43], which has led to the search for other active materials for glucose oxidation. Some of these drawbacks were overcome by modifying the surface of noble metals with different metal ad-layers [50-57]. However, the low sensitivity and toxicity of ad-metals such as Tl, Pb and Bi have hindered the development in this field [58]. Large amount of research work has been carried out using Au, Pt, Cu, Pt-Pb, boron doped diamond electrodes [59-72]. Porous material has interesting electrochemical properties find application in the glucose sensor [73-76].

Here, we have studied the porous Au NPs film for the determination glucose in the presence of interferences viz., ascorbic acid and uric acid. We have studied the glucose oxidation using cyclic voltammetry and chronoamperometry.

3.8.3.1 Cyclic Voltammetry Studies

Figure 29 shows the CV of porous Au NPs in the absence and presence of glucose solution taken in buffer solution of pH 7.0. In the absence of glucose solution CV shows a pair of peaks, which are characteristic redox peaks of the Au NPs which corresponds to the oxidation-reduction of gold oxides, a phenomenon known to occur at less negative potentials on the mesoporous gold surface [77]. This redox activity of Au NPs is used to oxidize the glucose. With increasing glucose concentration the oxidation current increases and the reduction current decreases correspondingly. The increasing oxidation current with glucose corresponds to the increasing surface oxidation of gold brought about by the addition of glucose. This process arises due to the oxidation of glucose by the surface oxides formed, which in turn is reduced. The positive

potential sweep increases the oxides which in turn are reduced during negative potential sweep. The process can be represented as

Au $\longrightarrow$ AuO (during positive potential scan)

AuO + Glucose $\longrightarrow$ Au + gluconic acid

3.8.3.2 Chronoamperometric Studies

Figure 30 shows the chronoamperometric response for the glucose. With increasing glucose concentration the current increases. The steady state for the glucose response reaches within 5 seconds. Figure 31 shows the current verses concentration plot. The linear response is obtained in the concentration range 1-12 mM as shown in the Figure 30.

3.8.3.3 Interference Studies

The oxidizable substances such as ascorbic acid (AA) and uric acid (UA) normally co-exist with glucose in real samples. In view of the physiological levels of glucose and the interfering agents, the amperometric response of the Au NPs modified electrode towards addition of 1 mM glucose and 0.1 mM electroactive molecules was examined. Figure 32 shows the chronoamperometry of glucose in the presence of AA, UA and the results are shown in the Table 8. Mesoporous gold has significant sensitivity for glucose, there is some interference by the addition of ascorbic acid and uric acid present at physiological concentration of 0.1 mM. However, considering the simplicity of this enzyme free method, the interference effect is not quite significant and may be accounted for any device level applications.

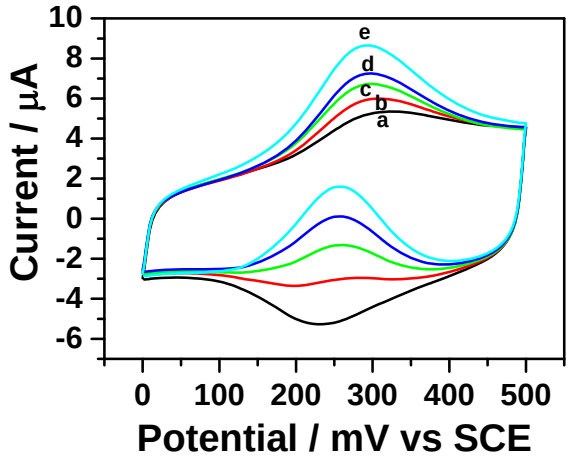

Figure 29. Shows the CV of Au NPs grown electrode using DT and KCl in (a) 0, (b) 2 mM, (c) 4 mM, (d) 6 mM, and (e) 8 mM glucose solution.

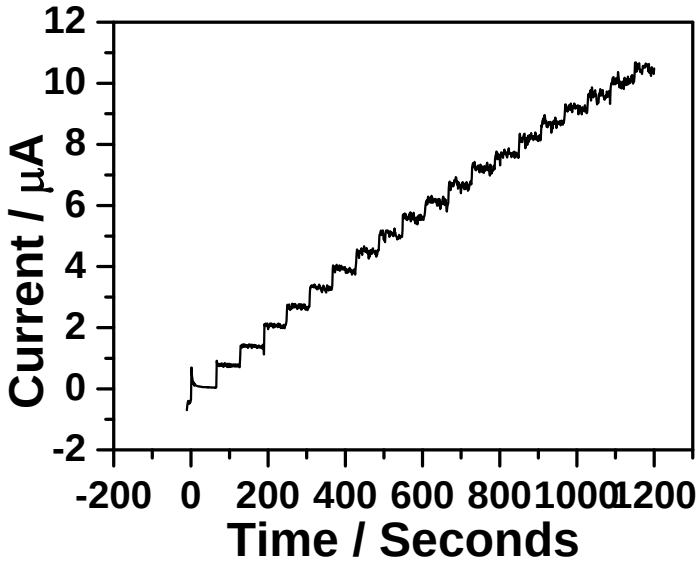

Figure 30. Chronoamperometry graph of Au NPs grown electrode using DT and KCl for the successive addition of 1 mM glucose

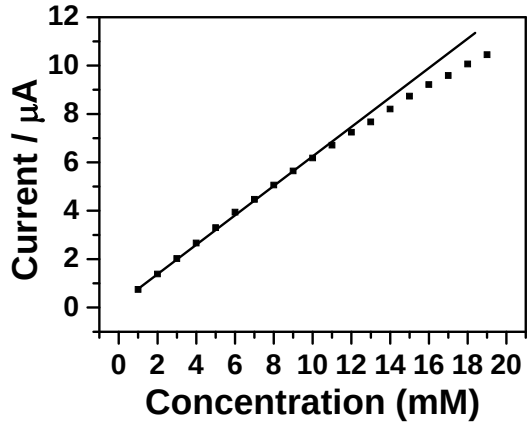

Figure 31. Calibration plot of Au NPs electrode for glucose

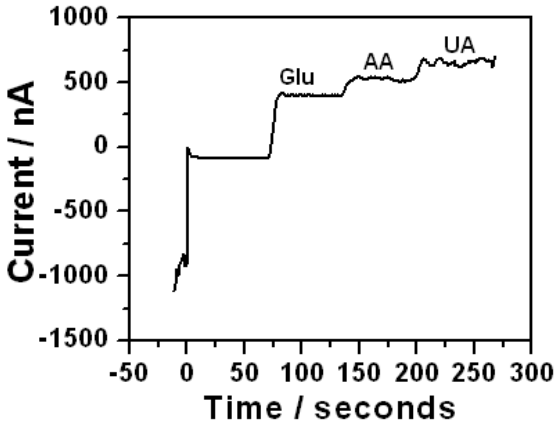

Figure 32. Interference effect for the glucose determination.

Substrate	Amperometric Current
Glucose (1mM)	485 nA
Ascorbic acid (0.1 mM)	134 nA
Uric acid (0.1 mM)	17 nA

Table 8. Amperometric current response for glucose, Ascorbic Acid and Uric Acid at Au NPs modified surface.

3.9 Conclusions

We have described in this chapter a method of preparing large surface area mesoporous gold on gold surface by a simple template free electrodeposition process. The deposition was carried out in the presence and also in the absence of the reducing agent $NaBH_4$. The Au NPs modified surface was characterized by SEM, EDAX, XRD and Cyclic Voltammetry. The SEM images clearly show the deposition of porous Au NPs on the cathode surface. AFM studies indicate the vertical growth of the nanoparticles on the electrode surface with porous geometry. Cyclic voltammetry of gold nanoparticles modified gold surface using oxide stripping method demonstrates that the material has a very high electrochemically active surface area. The real surface area increases with the time of deposition, which makes it possible to scale the process up for larger applications. We have studied the electrochemical properties of the *in situ* deposited high surface area Au NPs. Au NPs modified gold surface shows different diffusional behavior compared to the planar bulk gold electrode surfaces for electroactive species such as $K_4[Fe(CN)_6]$, $[Ru(NH_3)_6]Cl_3$, and dopamine. We have also studied the potential application of high surface area Au NP modified gold surfaces for dopamine detection in presence of ascorbic acid, glucose detection, and as a hydrogen evolution catalyst.

In the next chapter, we show that Au NPs can be deposited on platinum and graphite surfaces also and the mesoporous gold on Au, Pt, and graphite substrates which act can act as highly efficient electro-oxidation catalyst for methanol and ethanol oxidation in alkaline medium.

3.10 References

[1] M. Haruta, *Catal. Today*, **1997**, *36*, 153.

[2] M. Haruta, M. Date, *Appl. Catal. A* **2001**, *222*, 427.

[3] J. I. Brauman, P. Szuromi, *Science* **1996**, *273*, 855.

[4] G. S. Attard, P. N. Bartlett, N. R. B. Coleman, J. M. Elliot, J. R. Owen, J. H. Wang, *Science* **1997**, *278*, 838.

[5] M. C. Daniel, D. Astruc, *Chem. Rev.* **2004**, *104*, 293.

[6] S. C. Warren, L. C. Messina, L. S. Slaughter, M. Kamperman, Q. Zhou, S. M. Gruner, F. J. Disalvo, U. Wiesner, *Science* **2008**, *320*, 1748.

[7] M. E. Davis, *Nature* **2002**, *417*, 813.

[8] J. Erlebacher, M. J. Aziz, A. Karma, N. Dimitrov, K. Sieradzki, *Nature* **2001**, *410*, 450.

[9] H. Dong, X. Cao, *J. Phys. Chem. C* **2009**, *113*, 603.

[10] M. C. Dixon, T. A. Daniel, M. Hieda, D. M. Smilgies, M. H. W. Chan, D. L. Allara, *Langmuir* **2007**, *23*, 2414.

[11] Z. Borkowska, A. Tymosiak-Zielinska, R. Nowakowski, *Electrochim. Acta* **2004**, *49*, 613.

[12] C. D. Bain, E. B. Troughton, Y.-T. Tao, J. Evall, G. M. Whitesides, R. G. Nuzzo, *J. Am. Chem. Soc.* **1989**, *111*, 321.

[13] D. H. Nagaraju, V. Lakshminarayanan, *Langmuir* **2008**, *24*, 13855.

[14] J.O'M. Bockris, S. U. M. Khan, *Surface Electrochemistry, A molecular level approach*; Plenum Press: New York, **1993.**

[15] M. T. Reetz, W. Helbig, *J. Am. Chem. Soc.* **1994**, *116*, 7401.

[16] J. H. Gallego, C. E. Castellano, A. J. Calandra, A. J. Arvia, *J. Electroanal. Chem.* **1975**, *66*, 207.

[17] R. P. Brias, M. Hu, L. Qian, E. S. Lymar, J. F. Hainfeld, *J. Am. Chem. Soc.* **2008**, *130*, 975.

[18] T. G. Schaaff, M. N. Shafigullin, J. T. Khoury, I. Vezmar, R. L. Whetten, W. G. Cullen, P. N. First, C. Gutirrez-Wing, J. Ascensio, M. J. Jose-Yacamn, *J. Phys. Chem. B* **1997**, *101*, 7885.

[19] B. Wenzel, P. Lonnecke, E. Hey-Hawkins, *Eur. J. Inorg. Chem.* **2002**, 1761.

[20] S. Trasatti, O. A. Petrii, *Pure Appl. Chem.* **1991**, *63*, 711.

[21] R. Gulaboski, M. Chirea, C. M. Pereira, M. N. D. S. Cordeiro, R. B. Costa, A. F. Silva, *J. Phys. Chem. C* **2008**, *112*, 2428.

[22] I. Streeter, R. Baron, R. G. Compton, *J. Phys. Chem. C* **2007,** *111,* 17008.

[23] M. Chirea, C. M. Pereira, F. Silva, *J. Phys. Chem. C* **2007,** *111*, 9255.

[24] H. Luo, Z. Shi, N. Li, Z. Gu, Q. Zhuang, *Anal. Chem.* **2001**, *73*, 915.

[25] C. R. Raj, T. Okajima, T. Ohsaka, *J. Electroanal. Chem.* **2003**, *543*, 127.

[26] S. S. Kumar, J. Mathiyarasu, K. L. Phani, *J. Electroanal. Chem*. **2005**, *578*, 95.

[27] L. Zhang, X. J. Jiang, *J.* Electroanal. Chem. **2005,** *583*, 292.

[28] L. Lu, X. Wang, X. Lin, *Anal. Sci.* **2004,** *20*, 1131.

[29] X. Liu, F. Wang, S. Han, L. Shi, G. Xu, *Electroanalysis* **2010**, *22*, 963.

[30] G. J. Brug, M. Sluyters-Rehbach, J. H. Sluyters, A. Hemelin, *J. Electroanal. Chem.* **1984**, *181*, 245.

[31] A. Hamelin, M. J. Weaver, *J. Electroanal. Chem.* **1987**, *223*, 171.

[32] B. E. Conway, L. Bai, *Electrochim. Acta* **1986,** *31*, 1013.

[33] N. M. Markovic, B. N. Grgur, P. N. Ross, *J. Phys. Chem. B* **1997,** *101,* 5405.

[34] J. Perez, E. R. Gonzalez, H. Villullas, *J. Phys. Chem. B* **1998**, *102,* 10931.

[35] A. Hamelin, L. Stoicoviciu, S-C. Chang, M. J. Weaver, *J. Electroanal. Chem.* **1991,** *307***,** 183.

[36] F. Li, I. Ciani, P. Bertoncello, P. R. Unwin, J. Zhao, C. R. Bradbury, D. J. Fermin, *J. Phys. Chem. C* **2008**, *112,* 9686.

[37] G. Reach, G. S. Wilson, *Anal. Chem.* **1992**, *64*, 381A.

[38] L. S. Kuhn, *Electrochem. Soc. Interface* **1998**, *7*, 26.

[39] A. Heller, *Acc. Chem. Res*. **1990**, *23*, 128.

[40] Y. B. Vassilyev, O. A. Khazova, N. N. Nikolaeva, *J. Electroanal. Chem.* **1985**, *196,* 105.

[41] B. Beden, F. Largeaud, K. B. Kokoh, C. Lamy, *Electrochim. Acta* **1996,** 41, 701.

[42] R. Wilson, A. P. F. Turner, *Biosens. Bioelectron.* **1992,** *7,* 165.

[36] E. Shoji, M. S. Freund, *J. Am. Chem. Soc.* **2001,** *123,* 3383.

[43] Y. Sun, H. Buck, T. E. Mallouk, *Anal. Chem.* **2001,** *73,* 1599.

[44] M. Sakamoto, K. Takamura, *Bioelectrochem. Bioenerg.* **1982**, *9*, 571.

[45] I. G. Casella, M. Gatta, M. R. Guascito, T. R. I. Cataldi, *Anal. Chim. Acta* **1997,** *357,* 63.

[46] I. T. Bae, E. Yeager, X. Xing, C. C. Liu, *J. Electroanal. Chem.* **1991,** *309,* 131.

[47] R. R. Adzic, M. W. Hsiao, E. B. Yeager, *J. Electroanal. Chem.* **1989,** *260,* 475.

[48] M. W. Hsiao, R. R. Adzic, E. B. Yeager, *Electrochim. Acta* **1992,** *37*, 357.

[49] M. W. Hsiao, R. R. Adzic, E. B. Yeager, *J. Electrochem. Soc.* **1996,** *143,* 759.

[50] S.B. Aoun, Z. Dursun, T. Koga, G.S. Bang, T. Sotomura, I. Taniguchi, *J. Electroanal. Chem.* **2004,** *567,* 175.

[51] S. B. Aoun, G. S. Bang, T. Koga, Y. Nonaka, T. Sotomura, I. Taniguchi, *Electrochem. Commun.* **2003,** *5,* 317.

[52] G. Wittstock, A. Strübing, R. Szargan, G. Werner, *J. Electroanal. Chem.* **1998,** *444,* 61.

[53] X. Zhang, K.-Y. Chan, J.-K. You, Z.-G. Lin, A. C. C. Tseung, *J. Electroanal. Chem.* **1997,** *430,* 147.

[54] C. Jin, I. Taniguchi, *Mater. Lett.* **2007,** *61,* 2365.

[55] C. Jin, Z. Chen, *Synth. Met.* **2007,** *157*, 592.

[56] N. Xonoglou, G. Kokkinidis, *Bioelectrochem. Bioenerg.* **1984,** *12,* 485.

[57] G. Kokkindis, J. M. Leger, C. Lamy, *J. Electroanal. Chem.* **1988,** *242,* 221.

[58] F. Kurniawan, V. Tsakova, V. M. Mirsky, *Electroanalysis* **2006,** *18,* 1937.

[59] Y.-G. Zhou, S. Yang, Q.-Y. Qian, X.-H. Xia, *Electrochem. Commun.* **2009,** *11,* 216.

[60] X. Kang, Z. Mai, X. Zou, P. Cai, J. Mo, *Talanta* **2008,** *74,* 879.

[61] K. Zhao, S. Zhuang, Z. Chang, H. Songm, L. Dai, P. He, Y. Fang, *Electroanalysis* **2007,** *19,* 1069.

[62] X. Pang, D. He, S. Luo, Q. Cai, *Sens. Actuators B: Chem.* **2009,** *137,* 134.

[63] H.-F. Cui, J.-S. Ye, W.-D. Zhang, C.-M. Li, J. H. T. Luong, F.-S. Sheu, *Anal. Chim. Acta* **2007,** *594,* 175.

[64] C. Hui-Fang, Y. Jian-Shan, L. Xiao, Z. Wei-De, S. Fwu-Shan, *Nanotechnology* **2006,** 2334.

[65] Q. Xu, Y. Zhao, J. Z. Xu, J.-J. Zhu, *Sens. Actuators B: Chem.* **2006,** *114,* 379.

[66] J. H. Yuan, K. Wang, X. H. Xia, *Adv. Funct. Mater.* **2005,** *15,* 803.

[67] Y. Bai, W. Yang, Y. Sun, C. Sun, *Sens. Actuators B: Chem.* **2008,** *134,* 471.

[68] Y. Deng, W. Huang, X. Chen, Z. Li, *Electrochem. Commun.* **2008,** *10,* 810.

[69] Y. Bai, Y. Sun, C. Sun, *Biosens. Bioelectron.* **2008,** *24,* 579.

[70] Y. Lu, M. Yang, F. Qu, G. Shen, R. Yu, *Bioelectrochemistry* **2007,** *71,* 211.

[71] X. Zhang, D. Li, L. Bourgeois, H. Wang, P. A. Webley, *ChemPhysChem* **2009,***10,* 436.

[72] J. Zhao, L. Wu, J. Zhi, *Analyst* **2009,** *134,* 794.

[73] C.-H. Chou, J.-C. Chen, C.-C. Tai, I. W. Sun, J.-M. Zen, *Electroanalysis* **2008,** *20,* 771.

[74] S. Park, T. D. Chung, H. C. Kim, *Anal. Chem.* **2003,** *75*, 3046.

[75] Y.-Y. Song, D. Zhang, W. Gao, X.-H. Xia, *Chem. Eur. J.* **2005**, *11*, 2177.

[76] Y.-J. Lee, D.-J. Park, J.-Y. Park, Y. Kim, *Sensors* **2008,** *8*, 6154.

[77] L. D. Burke, A. J. Ahern, A. P. O'Mullane, *Gold Bulletin* **2002,** *35/1,* 3.